Nanoscale

Accepted Manuscript

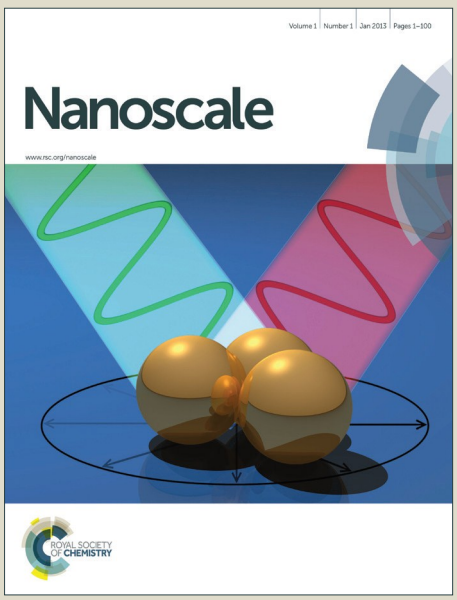

ROYAL SOCIETY OF CHEMISTRY

www.rsc.org/nanoscale

Nanoscale

COMMUNICATION

Freestanding Carbon-Coated CNT/Sn(O_2) Coaxial Sponges with Enhanced Lithium-Ion Storage Capability

Received 00th January 20xx,
Accepted 00th January 20xx

DOI: 10.1039/x0xx00000x

www.rsc.org/

Bin Luo,[a] Tengfei Qiu,[a] Bin Wang,[a] Long Hao,[a] Xianglong Li,[a] Anyuan Cao,[b] and Linjie Zhi*[a]

Carbon-coated, carbon nanotube (CNT)/tin (oxide) spongy coaxial nanostructures, CNT/Sn(O_2)@C, with large areal mass loadings have been developed by employing a three-dimensional CNT sponge as the backbone. The freestanding spongy coaxial nano-architecture demonstrates exceptional electrochemical characteristics of tin-based anode materials with appropriate structural engineering for energy storage application.

Lithium-ion batteries (LIBs) have attracted considerable attention for electrical energy storage with applications in portable electronic products, electric/hybrid vehicles, and stationary applications.[1] With the requirement of both high energy and power density performance for next-generation LIBs, great efforts have been made on design and fabrication of nanosized materials and structures because they provide high surface area and short diffusion paths for ionic and electronic conduction.[2-4] For anode applications, tin based materials have been considered as potential substitutes for current carbonaceous materials due to their high specific capacities (992 mAh g^{-1} for Sn, 782 mAh g^{-1} for SnO_2).[5, 6] However, anodes of such high capacity usually suffer severe capacity fading caused by both the aggregation of tin particles and the huge volume change during Li^+ insertion/extraction processes.[7] Nanostructures or nanocomposites are thus expected to play a significant role in next generation electrodes, exemplified by a wide variety of studies of tin based nanostructures as anodes.[8-20]

Carbon nanomaterials, such as carbon nanotubes (CNT) and graphene, are particularly attractive in combination with electrochemical active materials due to their excellent electronic conductivity, low density, and good mechanical and chemical stability.[21-26] For instance, composites consisted of CNT and SnO_2 have been reported by several groups to create CNT supported SnO_2 nanoparticles network.[27-38] Nevertheless, the exposed metal oxide nanoparticles on the CNT surface are still prone to disintegrate and, meanwhile, the volume expansion and aggregation of these active nanoparticles are difficult to avoid if content of active material is high. Furthermore, most of the reported CNT/SnO_2 composites were prepared using CNT as substrates for active component collection, then carbon black and polymer binders had to be used to lower the resistance and hold the electrodes together. Several recent studies demonstrated that the 3D CNT sponge network can be used as backbone in freestanding hybrid electrodes for energy storage application. For example, CNT/S and CNT/V_2O_5 hybrid sponges with improved electrochemical performance were developed through one step deposition methods.[39-41]

In the present work, we therefore designed a novel chemical strategy to create carbon coated CNT/tin (oxide) coaxial nanostructures, CNT/Sn(O_2)@C, for high-performance anode applications, in which 3D CNT sponge was employed as a structural backbone and freestanding nanostructured current collector. With excellent electronic conductivity and high porosity, the CNT sponge with high porosity in intimate contact with Sn based nanoparticles will profoundly reduce the time required for electron and ion transport during the charge-discharge process. Moreover, owing to the efficient protection of the carbon shells, the obtained CNT/Sn(O_2)@C manifests superior structural stability, leading to excellent cycling stability.

The overall synthetic procedure of CNT/Sn(O_2)@C is illustrated in **Fig. 1**a. Firstly, SnO_2 nanoparticles were synthesized via an *in situ* hydrolysis of corresponding metal salt and decorated on the pre-functionalized CNT sponge. Next, *in situ* polymerization and carbonization of glucose in the presence of CNT/SnO_2 sponge generated a glucose-derived carbon encapsulated product, namely CNT/SnO_2@C. Additionally, further thermal treatment of CNT/SnO_2@C at 550°C in H_2/Ar led to the reduction of SnO_2 nanoparticles, forming CNT sponge supported tin nanoparticles encapsulated by

[a] National Center for Nanoscience and Technology, Zhongguancun, Beiyitiao No. 11, Beijing, 100190, People's Republic of China
[b] Department of Materials Science and Engineering, College of Engineering, Peking University, Beijing 100871, People's Republic of China
Electronic Supplementary Information (ESI) available. See DOI: 10.1039/x0xx00000x

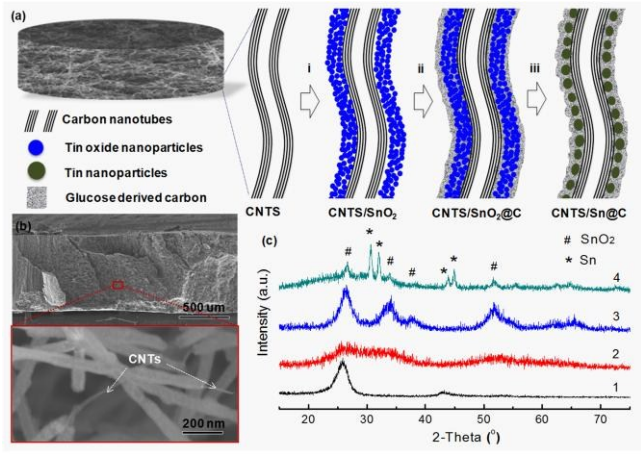

Fig. 1 a) Illustration of the formation of carbon coated CNT/Sn(O_2) sponge: (i) tin oxide (SnO_2) nanoparticles were firstly decorated on CNT sponge via a hydrolysis process; (ii) CNT/SnO_2 sponge was then coated with glucose-derived carbon through a hydrothermal method followed by a carbonization process; (iii) CNT/SnO_2@C was transformed into CNT/Sn@C through a thermal treatment under hydrogen/nitrogen atmosphere. b) SEM micrographs of 3D porous CNT/SnO_2@C sponge showing the coaxial structure of SnO_2@C shell conformally coated on CNTs. c) XRD patterns of (1) CNT, (2) CNT/SnO_2, (3) CNT/SnO_2@C, and (4) CNT/Sn@C sponges, respectively.

carbon shell, namely CNT/Sn@C. Detailed synthetic procedures are provided in the experimental section.

Fig. 1b and Fig. S1 show scanning electron microscopy (SEM) images at the cross section of a piece of a CNT/SnO_2@C sponge after incision. High magnification SEM micrograph demonstrates the uniform coaxial structure of SnO_2@C shell as a conformal coating on the surfaces of CNTs throughout the sponge, owing to the highly porous nature of the sponge. X-ray diffraction (XRD) experiments were carried out to reveal the composition and crystal structure evolution of CNT, CNT/SnO_2, CNT/SnO_2@C and CNT/Sn@C sponges during the synthetic process. As shown in Fig. 1c, the broad diffraction peaks for the CNT/SnO_2@C indicated the small crystal size of tetragonal rutile SnO_2 phase. All strong peaks of CNTS/Sn@C shown in Fig. 1c can be well indexed to β-Sn (JCPDS No. 04-0673), while the small peaks marked with # can be attributed to rutile SnO_2 (JCPDS No. 41-1445), which implies that a small amount of tin oxide are not reduced during the thermal treatment process.

The unique morphology and microstructure of as-synthesized CNT/SnO_2@C sponge were further characterized by field emission TEM and STEM. The marked area in **Fig. 2**a shows two independent CNTs are bound together by the glucose derived carbon, which is beneficial to the electron transport throughout the sponge electrode. Compared with the bare CNT (Fig. S2), the average diameter of the hybrid coaxial structure increased from ~20 nm to ~90 nm, that is, approximately 30 nm SnO_2 layer and 5 nm carbon shell were formed after the hydrolysis and hydrothermal process, respectively. From the high resolution TEM image as shown in Fig. 2b, the uniform distribution of tin oxide nanoparticles with a diameter of ~5 nm in the 1D porous carbon matrix composed of CNTs core and amorphous glucose derived carbon shell can

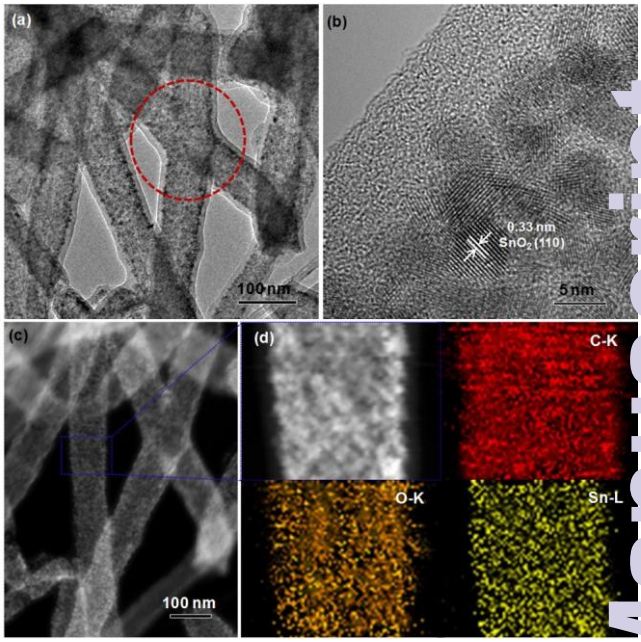

Fig. 2 a) TEM, b) HRTEM, c) STEM, and d) carbon, oxygen, and tin elem mapping images of the CNT/SnO_2@C sponge, demonstrating the uniform distribution of tin oxide nanoparticles with a diameter of ~5 nm in t hybrid coaxial structure. The marked area in a) shows two independen CNTs are bound together by the glucose derived carbon.

be observed. In comparison, without carbon coating, the ti oxide layer in CNT/SnO_2 exhibits a relative compact state with larger grain size after thermal annealing (Fig. S3). This resu indicates the existence of amorphous carbon matrix around tin oxide nanocrystals can efficiently suppress their grain growt during high temperature annealing process, which is also beneficial for buffering the volume change during th charge/discharge process.[10, 42] Fig. 2c, d show the STEM image and element mapping of CNT/SnO_2@C, further highlighting homogeneous distribution of tin oxide in the 1D carbon matrix. The outer dim shell and enclosed bright core shown in Fig can be distinctly assigned to amorphous carbon covers and inner tin oxide nanoparticles of the CNT/SnO_2@C, respectively, in agreement with HRTEM analysis.

The as-prepared CNT/SnO_2@C sponge were then furthe reduced into tin-based CNT/Sn@C composite by hydro assisted thermal reduction. SEM and TEM measurements wer carried out to determine its morphology and microstructure As shown in **Fig. 3**, it is observed that the obtained CNT/Sn@ maintains almost the same spongy morphology wit CNT/SnO_2@C. The encapsulated tin nanoparticles have a average diameter of 20 nm, which is larger than that of th SnO_2 nanoparticles before reduction. This can be ascribed t the low melting point of metallic tin that makes tin particle partially fused during the high temperature process Fortunately, the fusion process was efficiently suppressed an tin nanoparticles were well distributed in this case due to the existence of such unique CNT sponge-based carbon matri The HR-TEM image (Figure 3d) shows clear lattice fringes with a d-spacing of 0.29 nm, corresponding to the (200) plane of metallic tin (JCPDS card No. 04-0673). A small amount of S

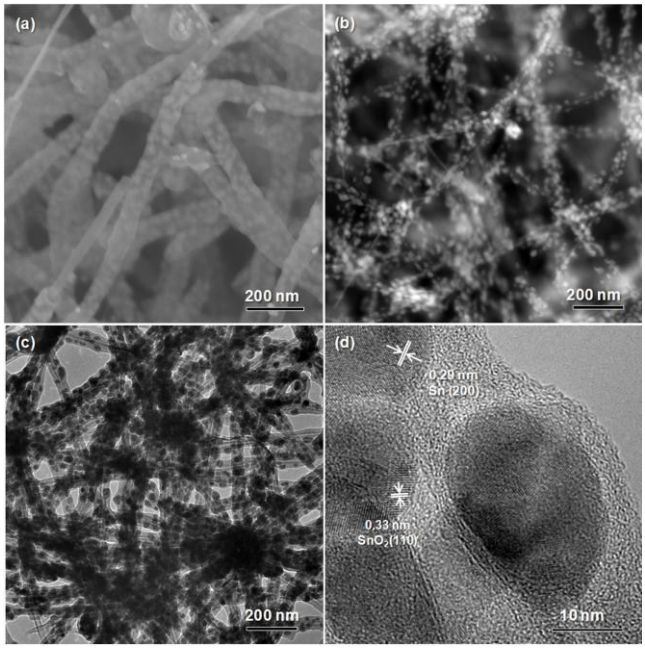

Fig. 3 a) SEM, b) STEM, and c, d) TEM images of the CNT/Sn@C sponge, demonstrating the uniform distribution of tin nanoparticles with an average diameter of ~20 nm in the hybrid coaxial structure.

nanophase with a d-spacing of 0.33 nm can also be observed, which is in agreement with XRD results.

In order to elucidate the effect of glucose-derived carbon coating on the reduction of tin oxide, here we compared two CNT/SnO_2@C samples with different carbon coating thickness, but with the same mass ratio of CNTs to SnO_2. To facilitate the later statement, the sponges before and after reduction are marked as CNT/SnO_2@C-1, CNT/SnO_2@C-2, and CNT/Sn@C-1, CNT/Sn@C-2 with the increasing carbon coating thickness, respectively. Thermogravimetric analysis (TGA) results reveal that the weight fraction of tin oxide in the CNT/SnO_2 composite is ca. 85.7% (Fig. S4). After carbon coating process, the glucose-derived carbon contents in CNT/SnO_2@C-1 and CNT/SnO_2@C-2 can be calculated from their TGA curves as 7.2%, 22.9%, respectively. From the TEM observations (Fig. 2b and S5), it is clearly to see the diameter change of CNT/SnO_2@C with the increasing carbon coating thickness. Interestingly, we found that the carbon coating thickness of CNT/SnO_2@C has an influence on the morphology of its reduced products. As we can see in Fig. 3, a well encapsulation of tin nanoparticles in CNT sponge-based carbon matrix, CNT/Sn@C-2, can be obtained with a proximately 5~7 nm carbon coating on the CNT/SnO_2 surfaces (CNT/SnO_2@C-2). If the carbon coating thickness was as thin as less than 3 nm (CNT/SnO_2@C-1, Fig. S5), the resultant would have a different morphology, in which tin nanoparticles with an average diameter larger than 30 nm are affixed on CNTs with or partially with very thin carbon coating layer on the particle surface (Fig. S6). These results further confirmed the important role of the carbon coating layer in the formation of well-confined tin nanoparticles.

The lithium ion storage capabilities of the obtained CNT/SnO_2@C sponges were evaluated by galvanostatic charge/discharge cycling in a cell with Li metal as coun electrodes. Before assembled in a coin cell battery, the abov spongy electrodes were compressed to increase their volum density. For instance, a typical spongy electrode with thickness of ~1.0 mm can be compressed into ~110 µm (Fi S7). After pressing in one direction, 3D porosity for electrolyte transport is preserved due to the highly porous nature of th sponge material. Unless otherwise mentioned, all the spongy electrodes in the text have a thickness of approximately 1 mm. To further investigate the effect of carbon coating and sponge thickness on the electrochemical performance of our CNT/SnO_2@C composite electrodes, we tested the cycling performance of CNT/SnO_2 without carbon coating an CNT/SnO_2@C electrodes with different thickness under th same conditions. **Fig. 4**a shows the cycling performance o these sponge electrodes with a cutoff voltage of 0.01-3.00 V and a current density of 100 mA g^{-1}. As we mentioned abo the CNT/SnO_2, CNT/SnO_2@C-1, CNT/SnO_2@C-2 samples with the same mass ratio of CNT to SnO_2 have different tin oxide contents due to their different carbon coating thickness. Higher content of active component in the hybrid electrode expected to have larger overall gravimetric specific capacity Thus, decreasing the thickness of carbon coating is favorable i this respect. Our results shown in Fig. 4a demonstrates tha CNT/SnO_2@C-1 sponge with a thinner carbon coating exhibi a higher reversible specific capacity up to ~1063 mAh g^{-1} than that of CNT/SnO_2@C-2 (~943 mAh g^{-1}). However, althoug CNT/SnO_2 with the highest SnO_2 content presents a higher initial discharge capacity than the other two samples, th cycling performance of CNT/SnO_2 electrode is very poor due to the absence of carbon coating. It can be observed that th capacity retention is significantly improved after carbon coating compared to cycling performance of CNT/SnO_2 an previously reported CNT-based SnO_2 composites.[27, 28, 32, 33, 35] Specifically, although the capacity still decays gradually c cycling, a high capacity of 854 mAh g^{-1} can be retained after 100 cycles at a current density of 100 mA g^{-1}.

Before carbon coating, the average mass loading of th SnO_2 on CNT sponge is ~4.0 mg cm^{-2} (See Supporting Information). According to the TGA results, the whole a weight of CNT/SnO_2@C-1, CNT/SnO_2@C-2 electrode including CNT and carbon coating shell, will be 5.0 and 6.1 m cm^{-2}. From this respect, the areal specific capacities o CNT/SnO_2@C-1 and CNT/SnO_2@C-2 electrode can b estimated to be ~5.3 mAh cm^{-2} and ~5.8 mAh cm^{-2} respectively. It should be noted that when a thicke CNT/SnO_2@C-2 electrode (~1.5 mm) was tested under th same current density, a slightly lower gravimetric specifi capacity of (~810 mAh g^{-1}) was obtained. However, thicke electrode means a higher areal mass loading of active materia and thus a much higher areal specific capacity of ~7.4 mAh cm $^{-2}$ was achieved for the thicker CNT/SnO_2@C-2 electrode with larger areal mass loading of ~9.2 mg cm^{-2}. Higher areal capacity are expected by using thicker CNT sponge based

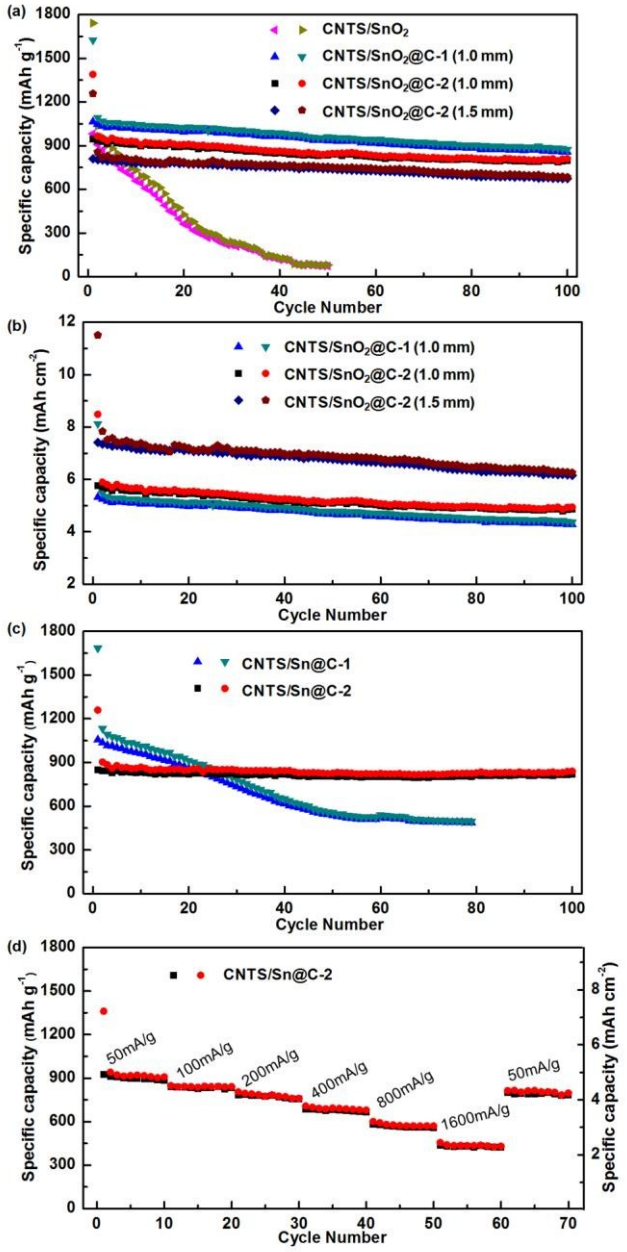

Fig. 4 a, b) Cycle performance of CNT/SnO_2, CNT/SnO_2@C-1, and CNT/SnO_2@C-2 with different electrode thickness at a current density of 100 mA g^{-1}. c) Cycle performance of CNT/Sn@C-1 and CNT/Sn@C-2 electrodes at a current density of 100 mA g^{-1} and d) the rate performance of CNT/Sn@C-2 at various current densities.

electrode and increasing the areal mass loading of the SnO_2 on CNT sponge.

The lithium storage properties of the obtained CNT/Sn@C sponges were also evaluated under the same electrochemical condition. Fig. 4c shows the comparison of the cycle performances of CNT/Sn@C-1 and CNT/Sn@C-2 at a current density of 100 mA g^{-1}. The later delivers a reversible capacity up to 847 mAh g^{-1} which could be maintained at 818 mAh g^{-1} after 100 cycles with a trace capacity loss. To our best knowledge, such electrochemical performance of CNT/Sn@C is

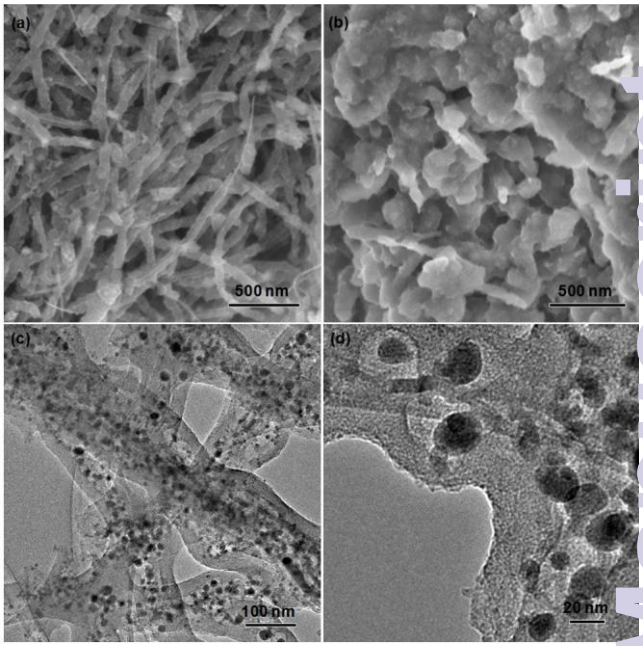

Fig. 5 SEM images of a) CNT/SnO_2@C and b) CNT/SnO_2 sponge electrodes after 100 charge/discharge cycles, respectively; c, d) TEM images of CNT/Sn@C-2 sponge electrode after 100 charge/discharge cycles.

superior or comparable to the literature reported carbon/tin nanocomposites.[9, 11, 18, 43-46] Although CNT/Sn@C-1 has a higher weight ratio of Sn than that of CNT/Sn@C-2, the specific capacity of CNT/Sn@C-1 decreases gradually from 1054.9 mAh g^{-1} to 485 mAh g^{-1} after 80 cycles. This might be understood in view of the structural features of the CNT/Sn@C-1 sponge (Fig. S6), in which Sn particles on CNTs are not well protected by carbon coating, leading to pulverization and agglomeration during cycling with severe capacity fading. Comparing with CNT/SnO_2@C-2, CNT/Sn@C-2 delivered a slightly lower first-discharge capacity of 1258 mAh g^{-1} (Fig. S8, S9) but with an similar initial coulombic efficiency of 67% (Fig. S10) which can be mainly attributed to the formation of SEI film on the electrode surface during the first discharge process. The rate performance of CNT/Sn@C-2 electrode was further inspected. Assuming that all the tin oxide in CNT/SnO_2@C-2 have been reduced into metallic tin, areal tin mass loading and the whole areal weight of CNT/Sn@C-2 electrode can be estimated as 3.2 and 5.3 mg cm^{-2}, respectively. And thus the areal capacities of CNT/Sn@C-2 electrode at various current densities can be estimated as shown in Fig. 4d. Remarkably, a high rate gravimetric/areal capacity up to 430 mAh g^{-1}/2.3 mAh cm^{-2} for CNT/Sn@C-2 at 1600 mA g^{-1} could be achieved.

The significantly improved electrochemical performance of CNT/Sn(O_2)@C sponges should indicate that little damage has happened at the electrodes. This was confirmed by SEM and TEM investigations of the composite sponge after repeated cycles. As shown in **Fig. 5**a, the spongy morphology with coaxial structure of CNT/SnO_2@C can be well remained, while the core-shell structure of CNT/SnO_2 without carbon coating have been seriously damaged after the repeated cycles (Fig. 5b). This might be attributed to the volume effect and

continuous formation of solid electrolyte interface (SEI) on tin oxide in CNT/SnO_2 which was directly immersed in the electrolyte. The evolution of the morphology and microstructure of CNT/Sn@C sponge during the charge/discharge processes were also investigated. TEM images of CNT/Sn@C-2 after 100 cycles (Fig. 5c, d) show that tin nanoparticles can be well confined in CNT supported carbon matrix and the void space in the carbon matrix caused by the volume change of tin-lithium alloy contribute greatly to the excellent cycling performance. It is reasonable to conclude that the exceptional performance of the CNT/Sn(O_2)@C composite sponges are attributed to their unique structures: (1) 3D carbon matrix composed of 1D CNT core and porous carbon shell with high surface area provides continuous path for both Li ions and electrons inside the composite sponges; (2) the highly porous CNT network together with the plastic carbon shell offers mechanical support to accommodate the stress associated with the large volume change of Sn based materials, thus alleviating pulverization; (3) the carbon matrix prevents Sn nanoparticles agglomeration efficiently upon prolonged charge/discharge cycling; and (4) nanopores or nanocavities in the Sn(O_2)@C shells also contribute positively to lithium ion storage.[47, 48] These composites are very promising as potential anode materials for LIBs even though the initial large capacity loss of these composite electrodes requires further improvement.

Conclusions

In summary, new types of tin based anode materials, namely CNT/Sn(O_2)@C, have been developed by employing porous, highly conductive 3D CNT sponge as backbone and glucose derived carbon as protecting shell. Owing to the 3D porous features inherited from CNT sponge as well as the efficient protection of the carbon shells, the prepared CNT/SnO_2@C manifests superior reversible capacity, and cycling stability compared with bare CNT/SnO_2 and the other recently reported CNT-based SnO_2 composites. Remarkably, an areal specific capacity as high as ~7.4 mAh cm^{-2} for CNT/SnO_2@C sponge with a large areal mass loading of ~9.2 mg cm^{-2} was achieved. Moreover, CNT/Sn@C with a uniform distributed tin nanoparticles has been obtained and exhibits a high reversible capacity up to 847 mAh g^{-1} which could be maintained at 818 mAh g^{-1} after 100 cycles as well as a high rate gravimetric/areal capacity up to ~430 mAh g^{-1}/2.3 mAh cm^{-2} at 1600 mA g^{-1}. It is expected that the present synthetic protocol can be further extended to build up various 1D coaxial nanomaterials with promising applications for energy conversion and storage.

Acknowledgements

Financial support from the Ministry of Science and Technology of China (No. 2012CB933403), the National Natural Science Foundation of China (Grant No. 21173057, 21273054), the Beijing Municipal Science and Technology Commission (Z121100006812003), and the Chinese Academy of Sciences is acknowledged.

Notes and references

1 J. M. Tarascon and M. Armand, *Nature*, 2001, **414**, 359.
2 A. L. M. Reddy, S. R. Gowda, M. M. Shaijumon and P. M. Ajayan, *Adv. Mater.*, 2012, **24**, 5045.
3 M. G. Kim and J. Cho, *Adv. Funct. Mater.*, 2009, **19**, 1497.
4 P. Poizot, S. Laruelle, S. Grugeon, L. Dupont and J. M. Tarascon, *Nature*, 2000, **407**, 496.
5 I. A. Courtney and J. R. Dahn, *J.Electrochem. Soc.*, 1997, **144**, 2045.
6 Y. Idota, T. Kubota, A. Matsufuji, Y. Maekawa and T. Miyasaka, *Science*, 1997, **276**, 1395.
7 B. Veeraraghavan, A. Durairajan, B. Haran, B. Popov and R. Guidotti, *J. Electrochem. Soc.*, 2002, **149**, A675.
8 K. T. Lee, Y. S. Jung and S. M. Oh, *J. Am. Chem. Soc.*, 2003, **125**, 5652.
9 G. Derrien, J. Hassoun, S. Panero and B. Scrosati, *Adv. Mater.*, 2007, **19**, 2336.
10 X. W. Lou, C. M. Li and L. A. Archer, *Adv. Mater.*, 2009, **21**, 25
11 W. M. Zhang, J. S. Hu, Y. G. Guo, S. F. Zheng, L. S. Zhong, W. G. Song and L. J. Wan, *Adv. Mater.*, 2008, **20**, 1160.
12 Y. Yu, L. Gu, C. L. Wang, A. Dhanabalan, P. A. van Aken and J. Maier, *Angew. Chem. Int. Ed.*, 2009, **48**, 6485.
13 B. Luo, B. Wang, X. Li, Y. Jia, M. Liang and L. Zhi, *Adv. Mater.*, 2012, **24**, 3538.
14 B. Luo, B. Wang, M. Liang, J. Ning, X. Li and L. Zhi, *Adv. Mater.*, 2012, **24**, 1405.
15 G. L. Cui, Y. S. Hu, L. J. Zhi, D. Q. Wu, I. Lieberwirth, J. Maier and K. Mullen, *Small*, 2007, **3**, 2066.
16 J. Liang, X.-Y. Yu, H. Zhou, H. B. Wu, S. Ding and X. W. Lou, *Angew. Chem. Int. Ed.*, 2014, **53**, 12803.
17 L. Zhang, H. B. Wu, B. Liu and X. W. Lou, *Energ. Environ. Sci.*, 2014, **7**, 1013.
18 P. Chen, F. Wu and Y. Wang, *ChemSusChem*, 2014, **7**, 1407.
19 Y. Gu, F. Wu and Y. Wang, *Adv. Funct. Mater.*, 2013, **23**, 893.
20 Y. Q. Zou and Y. Wang, *ACS Nano*, 2011, **5**, 8108.
21 B. J. Landi, M. J. Ganter, C. D. Cress, R. A. DiLeo and R. P. Raffaelle, *Energ Environ. Sci.*, 2009, **2**, 638.
22 A. Marschilok, C. Y. Lee, A. Subramanian, K. J. Takeuchi and E. S. Takeuchi, *Energ Environ. Sci.*, 2011, **4**, 2943.
23 M. H. Liang and L. J. Zhi, *J. Mater. Chem.*, 2009, **19**, 5871.
24 B. Luo, S. Liu and L. Zhi, *Small*, 2012, **8**, 630.
25 B. Luo and L. J. Zhi, *Energ. Environ. Sci.*, 2015, **8**, 456.
26 B. Luo, Y. Fang, B. Wang, J. Zhou, H. Song and L. Zhi, *Energ. Environ. Sci.*, 2012, **5**, 5226.
27 G. Chen, Z. Y. Wang and D. G. Xia, *Chem. Mater.*, 2008, **20**, 6951.
28 Z. H. Wen, Q. Wang, Q. Zhang and J. H. Li, *Adv. Funct. Mater.*, 2007, **17**, 2772.
29 H. X. Zhang, C. Feng, Y. C. Zhai, K. L. Jiang, Q. Q. Li and S. S. Fan, *Adv. Mater.*, 2009, **21**, 2299.
30 H. K. Zhang, H. H. Song, X. H. Chen, J. S. Zhou and H. J. Zhang, *Electrochimica Acta*, 2012, **59**, 160.
31 J. H. Lee, B. S. Kong, S. B. Yang and H. T. Jung, *J. Power Sources*, 2009, **194**, 520.
32 Z. Y. Wang, G. Chen and D. G. Xia, *J. Power Sources*, 2008, **184**, 432.

33 G. M. An, N. Na, X. R. Zhang, Z. J. Miao, S. D. Miao, K. L. Ding and Z. M. Liu, *Nanotechnology*, 2007, **18**, 435707.
34 S. D. Seo, G. H. Lee, A. H. Lim, K. M. Min, J. C. Kim, H. W. Shim, K. S. Park and D. W. Kim, *RSC Adv.*, 2012, **2**, 3315.
35 S. J. Ding, J. S. Chen and X. W. Lou, *Adv. Funct. Mater.*, 2011, **21**, 4120.
36 Y. H. Jin, K. M. Min, S. D. Seo, H. W. Shim and D. W. Kim, *J. Phys. Chem. C*, 2011, **115**, 22062.
37 J. G. Ren, J. B. Yang, A. Abouimrane, D. P. Wang and K. Amine, *J. Power Sources*, 2011, **196**, 8701.
38 L. Noerochim, J. Z. Wang, S. L. Chou, D. Wexler and H. K. Liu, *Carbon*, 2012, **50**, 1289.
39 X. Y. Chen, H. L. Zhu, Y. C. Chen, Y. Y. Shang, A. Y. Cao, L. B. Hu and G. W. Rubloff, *ACS Nano*, 2012, **6**, 7948.
40 L. B. Hu, H. Wu, Y. F. Gao, A. Y. Cao, H. B. Li, J. McDough, X. Xie, M. Zhou and Y. Cui, *Adv. Energy Mater.*, 2011, **1**, 523.
41 X. C. Gui, J. Q. Wei, K. L. Wang, A. Y. Cao, H. W. Zhu, Y. Jia, Q. K. Shu and D. H. Wu, *Adv. Mater.*, 2010, **22**, 617.
42 X. W. Lou, J. S. Chen, P. Chen and L. A. Archer, *Chemistry of Materials*, 2009, **21**, 2868.
43 J. Hassoun, G. Derrien, S. Panero and B. Scrosati, *Adv. Mater.*, 2008, **20**, 3169.
44 D. Deng and J. Y. Lee, *Angew. Chem. Int. Ed.*, 2009, **48**, 1660.
45 J. L. Tirado, R. Santamaria, G. F. Ortiz, R. Menendez, P. Lavela, J. M. Jimenez-Mateos, F. J. G. Garcia, A. Concheso and R. Alcantara, *Carbon*, 2007, **45**, 1396.
46 Y. Wang, M. Wu, Z. Jiao and J. Y. Lee, *Chem. Mater.*, 2009, **21**, 3210.
47 X. W. Lou, Y. Wang, C. L. Yuan, J. Y. Lee and L. A. Archer, *Adv. Mater.*, 2006, **18**, 2325.
48 Y. Wang, H. C. Zeng and J. Y. Lee, *Adv. Mater.*, 2006, **18**, 645.